 

https://doi.org/10.1070/QEL18039

# Amplification of laser radiation at the edge of the KrF (B–X) spectral line

S.A. Yampolskaya, A.G. Yastremskii, Yu.N. Panchenko, A.V. Puchikin

*Abstract.* **We report the results of experimental and numerical studies of the KrF electric discharge amplifier operating on a mixture of He–Kr–$F_2$ gases. The possibility of expanding the short-wavelength spectral region of the induced radiation tuning at the B–X transition of the KrF molecule by removing the inverse population from the upper vibrational states of the electronic B level is shown. It is demonstrated that at the boundary of the active medium gain contour, the measured gain at a wavelength of 246.8 nm is 0.053 cm$^{-1}$. Using the developed 1D model of the KrF electric discharge amplifier, it is shown that when the active medium is excited by a pump pulse with a specific peak power of ~10 MW cm$^{-3}$, the gain in this spectral region is due to a longer relaxation time of the population of excimer molecules from the upper vibrational levels compared with the characteristic time of their production.**

***Keywords:*** *electric discharge KrF laser, vibrational relaxation, numerical simulation.*

## 1. Introduction

Apart from the high energy characteristics of excimer lasers, one of their attractive features is the large width of the spectral gain line of the active transition. This opens up the possibility of developing high-power sources of coherent UV radiation with wavelength tuning. In one of the first papers dedicated to this problem [1], a simple scheme for tuning an optical resonator using a quartz prism in electric-discharge ArF and KrF lasers made it possible to obtain an operating wavelength range with a width of ~2 nm. However, the obtained low values of the radiation energy cast doubt on the possibility of practical application of the optical wavelength tuning method for excimer lasers. Currently, this problem is solved by injecting low-power narrow-band radiation into a high-power excimer laser that acts as an amplifier. The researchers' interest in the design of such amplifiers is primarily related to the progress in the field of laser spectroscopy and detection of substances in the atmosphere and on the surface of bodies in which such systems are used as sources of probe pulses [2].

Analysis of the papers published during the period of research on rare-gas halide lasers shows that the main part of energy passes through the reservoir of the upper vibrational energy levels of excimer molecules before moving to the lower levels [3–5]. The study of the processes of vibrational relaxation of excimer molecules was carried out most intensively in the 1980s–1990s and was mainly theoretical in nature. Phenomenological models were proposed in which the set of all the vibrational levels was considered as a single state, and the interaction of the ground and excited states was described using generalised rates [6–8]. Also were put forth the models in which kinetic equations were solved that take into account collisional transitions between vibrational levels [5, 9, 10], as well as models in which the vibrational relaxation of excimer molecules was considered as motion in the space of vibrational energy [11, 12]. The use of these models made it possible to explain a number of physical effects and predict new ones. Nevertheless, two important questions remained unexplored: the effect of the conditions of excitation of the active medium on the distribution of excimer molecules over vibrational levels and the quantitative description of the generation of laser radiation from vibrationally excited levels of excimer molecules.

This paper presents experimental and theoretical results of studying the amplification of UV radiation with a wavelength of 246.8 nm in the KrF electric-discharge amplifier with a ~30-ns duration of the pulse exciting the active medium. Theoretical results were obtained using a 1D model of an electric-discharge KrF laser, in which, together with the currents and voltages in the excitation scheme and the concentrations of particles formed in the discharge plasma, the characteristics of induced radiation from the six lower vibrationally excited levels of the KrF molecule(B) are calculated.

## 2. Experimental setup and experimental results

Experimental studies were performed on an electric-discharge KrF laser of the ELF series, with a pulse energy of up to 1 J and a pulse repetition rate of up to 100 Hz, developed at HCEI SB RAS [13]. The laser was pumped from a Fitch generator (*LC* inverter) with recharging to the discharge capacitance (Fig. 1). Automatic preionisation of the discharge gap was carried out by UV radiation from spark dischargers installed in the first loop of the electric circuit. A TPI1-10k/20 thyratron was used as a switch. The charging voltage was varied in the range of 18–24 kV. The laser used a He : Kr : $F_2$ = 2300 : 100 : 2.5 gas mixture at a total pressure of 2.4 atm. The compact arrangement of the laser chamber and $C_3$ capacitances made it possible to obtain low inductance $L_4$ (~4 nH) in the second circuit. This ensured a short duration and high current (up to 90 kA) of the pump pulse. Profiled electrodes with a length of 45 cm, located at a distance of 2.55 cm from

**S.A. Yampolskaya, A.G. Yastremskii, Yu.N. Panchenko, A.V. Puchikin** Institute of High Current Electronics, Siberian Branch, Russian Academy of Sciences, prosp. Akademicheskii 2/3, 634055 Tomsk, Russia; e-mail: s_yampolskaya@yahoo.com

Received 8 November 2021; revision received 24 January 2022
*Kvantovaya Elektronika* **52** (5) 437–442 (2022)
Translated by M.A. Monastyrskiy

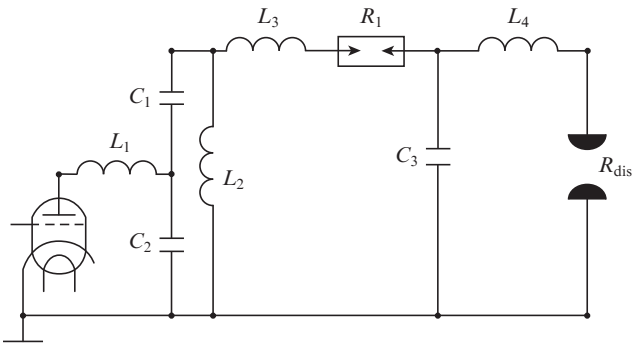


**Figure 1.** Electrical circuit of KrF laser excitation: $C_1$ = 49 nF, $C_2$ = 98 nF, $C_3$ = 34 nF; $L_1$ = 20 nH, $L_2$ = 100 nH, $L_3$ = 90 nH, $L_4$ = 4 nH; $R_1$ is the spark discharger resistance; $R_{dis}$ is the discharge resistance.

each other, made it possible to maintain the discharge width equal to ~0.8 cm during the entire excitation pulse. The laser chamber had $CaF_2$ windows installed at an angle of 5° to the optical axis.

To conduct experiments to determine the quantitative characteristics of the active medium at the short-wavelength edge of the spectral gain contour of the KrF amplifier, we used radiation with a wavelength of 246.8 nm, an energy of 0.1 mJ, and a pulse duration of 8 ns, obtained after the SRS conversion of the fourth harmonic of the Nd:YAG laser (266 nm) in methane. This anti-Stokes beam was isolated from the total light flux of Stokes pulses using an isosceles quartz prism with an apex angle of 58°. Next, this pulse passed through a lens telescope providing a given angular orientation of the probe beam and matching its aperture with the active medium of the amplifier. Circular diaphragms with a diameter of 0.7 cm were installed in front of the input and output of the amplifier, forming the optical axis in the active medium of the amplifier, along which the probe beam propagated. The radiation parameters after passing the amplifier were measured using wedge-shaped quartz plates, which diverted radiation to an Ocean optics HR4000 spectrometer, a FEK22 SPU photodiode, and a Gentec-EO calorimeter.

Figure 2 shows the radiation spectrum of the probe beam passed through the amplifier and the spontaneous emission of the active medium of the amplifier for the charging voltage

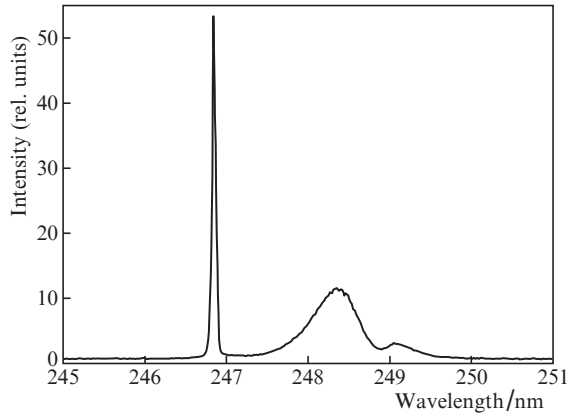


**Figure 2.** Recorded emission spectrum of the active medium of the KrF amplifier for a He:Kr:$F_2$ = 2300:100:2.5 mixture at a pressure of 2.5 atm and a charging voltage of $U_0$ = 22 kV. The initial pulse enters the active medium 10 ns after the discharge gap breakdown.

$U_0$ = 22 kV. The probe beam entered the active medium in $\Delta t$ = 10 ns, following the discharge gap breakdown. It can be seen that the probe radiation wavelength falls on the spectral band boundary of the spontaneous noise of the B–X transition of the KrF molecule.

The intensity ratio of the input ($I_0$) and amplified ($I$) pulses was used to estimate the small-signal gain without taking into account the absorption coefficient of the medium: $g = \ln(I/I_0)/L$, where $L$ is the active medium length. The maximum gain of $g$ = 0.052 $cm^{-1}$ was obtained in this series of experiments for a charging voltage of $U_0$ = 22 kV and a delay time of $\Delta t$ = 30 ns. Beam energy measurements for these conditions showed that, with the amplifier turned off, the radiation that passed through the optical system had an energy of 0.1 mJ; while after the amplifier was turned on, the energy increased to 1.5 mJ. In this case, an amplified spontaneous radiation energy of ~0.4 mJ was recorded. The active medium gain estimated from the ratio of the energies of the input and amplified beams was 0.053 $cm^{-1}$.

## 3. Model

To explain the experimental results obtained, we developed a 1D model of an electric-discharge KrF laser based on a Kr–$F_2$ gas mixture with He or Ne as a buffer gas, which made it possible to simulate both the radiation amplification process in the single-pass regime and the lasing regimes in a plane-parallel resonator. The discharge was considered homogeneous throughout the volume. The formation of the induced radiation flux was calculated along the active medium length. In numerical simulation of laser operation, the rate equations for the concentrations of plasma components were solved together with the system of equations for the electrical excitation circuit, the Boltzmann equation for the electron energy distribution function, and the radiation transfer equation describing the development of a photon avalanche in the resonator. The form of equations and methods for calculating the entire system of equations were discussed in detail in [14]. There is also a list of kinetic reactions included in the model for mixtures with Ne as a buffer gas.

When using the model for working mixtures with He, we took into account the same processes as for mixtures with Ne. Data from [15–18] were used to determine the dependences of the cross sections of He excitation and ionisation processes on the electron energy, as well as the rate constants of reactions involving He. As a result, the kinetic model describes the change in the concentrations of electrons $n_e$, excited He and Ne atoms (states 3s and 3p are separated), Kr (5s, 5p and the effective level combining states 4d and 6s), F (3s and 3p), as well as the concentrations of vibrationally excited $F_2$ molecules (molecules with vibrational numbers $v$ = 0, 1, 2, 3) and $He^+$, $Ne^+$, $Kr^+$, $F^+$, $F^-$, $Kr_2^+$, $He_2^+$, $Ne_2^+$, $NeKr^+$, and $HeKr^+$ ions.

Even in the first works devoted to excimer lasers [10, 19], it was noted that both as a result of ion–ion recombination reactions and in processes involving excited particles, excimer molecules are produced at the upper vibrationally excited levels. The population of lower vibrational levels is a consequence of vibrational quenching in collisions with other particles. Due to the finite rate of vibrational relaxation, only part of the excimer molecules participates in the processes of induced emission, which occurs mainly from the ground vibrationally unexcited level. In order to make allowance for this effect and not to complicate the model by detailed calculation

of relaxation processes, which is important in numerical simulation of the operation of real laser installations, a four-level excimer molecule model was used in [20, 21]. The zero and all combined vibrationally excited levels for B and C states were separated. Collisional transitions between these levels were described by generalised rates. The selection of vibrational relaxation and BC exchange rates made it possible to accurately predict the output characteristics of lasers, including the pulse shape and the delay time of its front relative to the pump current pulse.

In order to use this approach to study the possibility of obtaining induced radiation at the B–X transition from vibrationally excited states, we have expanded the representation of the KrF(B) state. As many as 10 lower vibrational levels were included (Fig. 3). The variables $k_{ij}$ and $k_{ji}$ determined the rates of forward and backward transitions between the vibrational levels $i$ and $j$ of KrF molecules as a result of their collisions with heavy particles and electrons. Since the energy difference between neighbouring levels for lower vibrational levels is $\sim 1-2\ k_B T$ (thermal quantum energy), we assumed that transitions are only possible between neighbouring levels $j = i - 1$. The rate constants of vibrational relaxation and BC exchange for different vibrational levels of KrF(B) and KrF(C) states, which were used in the model, are presented in Table 1.

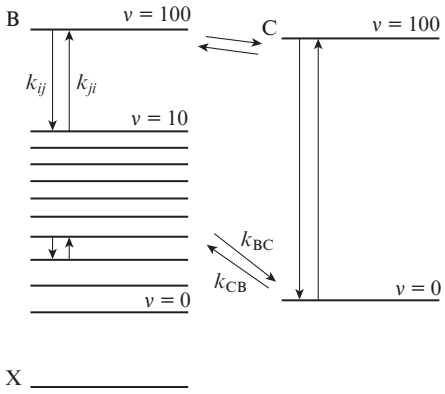


**Figure 3.** Level model of the KrF molecule.

To confirm the efficiency of the proposed model, we relied on the following: the coincidence of the simulation results with the results of the experiment for a KrF laser on the B–X transition from the ground state ($\lambda = 248.6$ nm), the characteristic time obtained in the model for establishing the equilibrium distribution of excimer molecules in vibrational levels, corresponding to $\sim 10$ collisions in an isolated system of levels, and agreement with experimental results in terms of the calculated gain for radiation with a wavelength of 246.8 nm.

Figure 4 shows both experimental and calculated dependences of the radiation energy of an electric-discharge KrF laser with an excitation pulse duration of $\sim 30$ ns on the charging voltage. The laser setup, initial conditions, and experimental technique are described in more detail in work [14]. The calculations assumed that the discharge has the same width in all excitation regimes. The result of spark preionisation was simulated by a volume-homogeneous initial electron concentration of $10^8$ cm$^{-3}$. Figure 4 shows good agreement between the calculation and experimental results within a confidence interval of 6%.

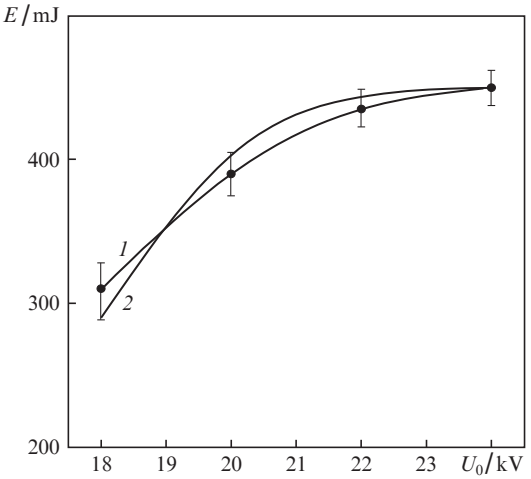


**Figure 4.** (*1*) Experimental and (*2*) calculated dependences of the laser energy $E$ on the charging voltage $U_0$ for a gas mixture Ne : Kr : $F_2$ = 3200 : 110 : 4.

**Table 1.** Vibrational relaxation and BC-exchange reactions used in the model [M is a particle (Kr, Ne, He, $F_2$ or electron)].

| Process | Rate constant/ cm$^{-3}$ | Paper |
|---|---|---|
| KrF(B,$v$) + M → KrF(C,$v$) + M | $5 \times 10^{-10}$ | [7] |
| KrF(C,$v$) + M → KrF(B,$v$) + M | $3.5 \times 10^{-10}$ | [7] |
| KrF(B,$v$) + Kr → KrF(B,$v-1$) + Kr | $8 \times 10^{-11}$ | [6] |
| KrF(B,$v$) + (He, Ne) → KrF(B,$v-1$) + (He, Ne) | $1 \times 10^{-11}$ for $v \leqslant 10$<br>$5 \times 10^{-11}$ for upper levels | [9]<br>[9] |

The rates of backward transitions from the vibrational level $j = v - 1$ to the level $i = v$ were determined from the Boltzmann distribution over the vibrational levels:

$$k_{ji} = k_{ij} \exp\left(-\frac{\Delta\varepsilon_{ij}}{kT}\right), \quad (1)$$

where $k_{ij}$ is the rate constant of the direct process, and $\Delta\varepsilon_{ij}$ is the energy difference between the levels.

## 4. Characteristic time of establishing the equilibrium distribution of excimer molecules over vibrational excitation levels

Model calculations were carried out to determine the characteristic times for the establishment of an equilibrium distribution over vibrational levels. It was assumed that at the time

moment $t = 0$, the total population of KrF excimer molecules was concentrated at the upper vibrational levels and amounted to $10^{15}$ cm$^{-3}$. Over time, as a result of collisions with other particles, lower vibrational levels were populated. Figure 5 shows the time dependences of the populations of the vibrational levels of the KrF(B) state at a helium buffer gas pressure of 2.5 atm. It can be seen that a stationary distribution over vibrational levels is established after 6 ns, for which 80% of KrF molecules are at a zero vibrational level.

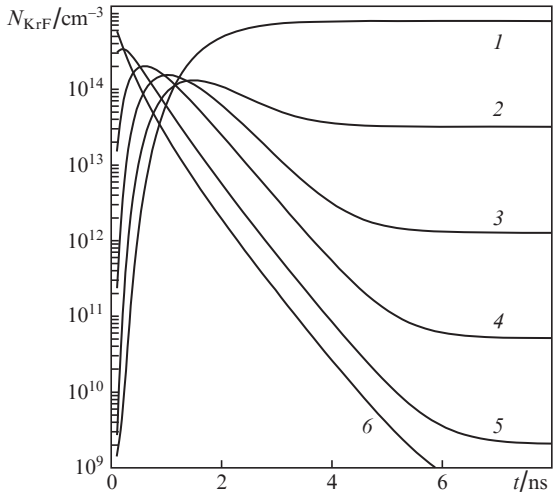


**Figure 5.** Time dependences of the concentration of KrF(B) molecules at vibrational levels $v$ = (*1*) 0, (*2*) 2, (*3*) 4, (*4*) 6, (*5*) 8 and (*6*) 100.

The time to reach the equilibrium distribution depends largely on the operating pressure. Figure 6 shows the dependence of the equilibrium distribution establishment time $\tau$ on the helium pressure. With increasing pressure, the equilibrium distribution is reached in less time. The characteristic times in the pressure range from 1 to 4 atm are 10–3 ns.

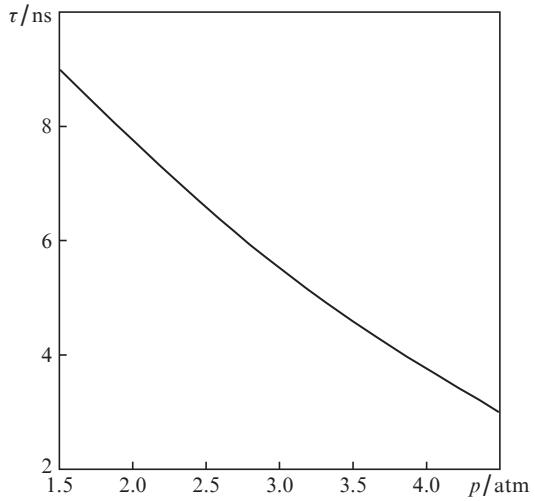


**Figure 6.** Dependence of the equilibrium distribution establishment time $\tau$ on the pressure $p$ of the buffer gas He. The ratio $Kr:F_2 = 100:4$ remained constant.

## 5. Distribution of excimer molecules over vibrational levels during pulsed excitation of the medium

In works [22, 23] relying on the assumption of the equilibrium distribution of excimer molecules over the levels of vibrational excitation, theoretical spontaneous emission spectra were obtained, which are in good agreement with the experimentally measured ones. The question arises whether this assumption is suitable for conditions of pulsed excitation of an active medium by an electric discharge with a duration of the order of tens of nanoseconds.

The results discussed below were obtained under conditions corresponding to the experiment with helium as a buffer gas (see Section 2). The discharge current and the voltage on the discharge plasma and the peaking capacitance $C_3$ for the charging voltage $U_0 = 22$ kV are shown in Fig. 7. The electric excitation circuit provides a pump pulse with a FWHM of ~30 ns and a specific maximum power of 10 MW cm$^{-3}$.

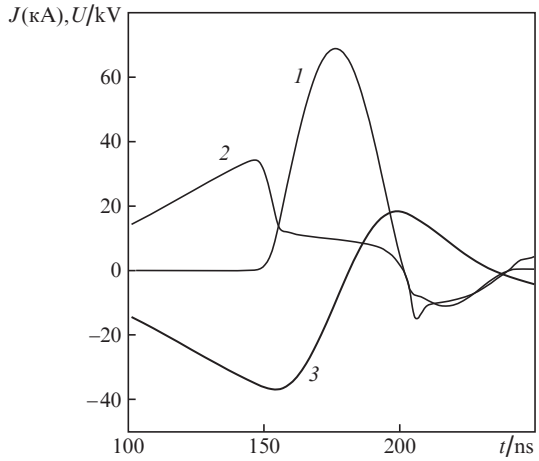


**Figure 7.** Time dependences of (*1*) the discharge current $J$ and (*2*, *3*) voltage $U$ at (*2*) the discharge gap and (*3*) capacitance $C_3$.

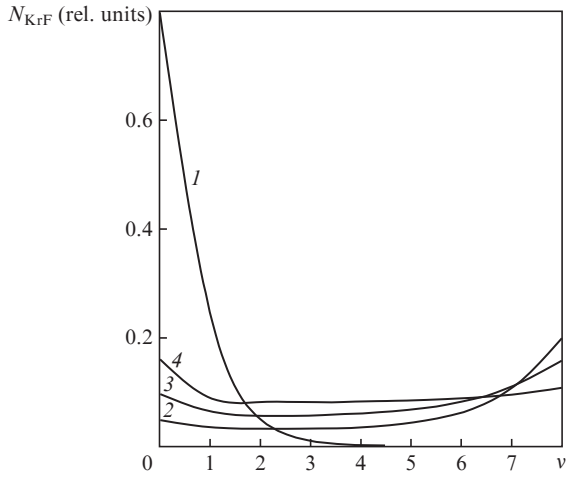


**Figure 8.** (*1*) Equilibrium distribution of the concentration of KrF(B) molecules over the vibrational levels $v$ and (*2*–*4*) similar distributions at the discharge current maximum at helium pressures (*2*) 1.4, (*3*) 2.4, and (*4*) 4.5 atm.

Figure 8 shows the distributions of KrF(B) molecules over vibrational levels, which are reached at a maximum of the discharge current pulse at various buffer gas pressures. Concentrations are normalised to the total number of KrF(B) molecules. For comparison, the same Figure shows the equilibrium distribution over vibrational levels for KrF(B). It can be seen that in the equilibrium state of the system of vibrational levels, 99% of the KrF(B) molecules populate the first four levels, and 80% of all KrF(B) molecules are in the state with $v = 0$. However, under pulsed pumping, all vibrational levels of KrF(B) molecules are populated, and at pressures of 1–2 atm, the population of the upper vibrational levels exceeds the ground state population. Despite the fact that as the pressure increases, more and more of the produced KrF molecules manage to move to the ground level, the equilibrium distribution is not achieved even at a pressure of 4 atm.

## 6. Amplification of radiation with a wavelength of 246.8 nm

When simulating radiation amplification at a wavelength of 246.8 nm, the equation for the radiation flux $F$

$$\frac{\partial F(l,t)}{\partial l} + \frac{1}{c}\frac{\partial F(l,t)}{\partial t} = \\ = F(l,t)\left(\sum_v \sigma_v N_{\mathrm{KrF}v} - \sum_k \sigma_k N_k\right) + \Omega N_{\mathrm{KrF}v}/\tau_v, \qquad (2)$$

was solved numerically, where $l$ is the distance along the amplifier axis; $c$ is the speed of light; $\sigma_k$ are the cross sections of radiation absorption by the particles of the $k$th type; $N_k$ is the concentration of such particles; $\tau_v$, $\sigma_v$ and $N_{\mathrm{KrF}v}$ are the spontaneous lifetime, the cross section of induced radiation, and the population for the vibrational level $v$ of the KrF(B) molecule, respectively; and $\Omega$ is the fraction of spontaneous photons moving along the direction of laser photon propagation. Based on the results of work [10], we assumed that the radiation with $\lambda = 246.8$ ns interacts with vibrational levels $v = 5$ and 6, while the cross sections of the induced radiation were estimated as 2.2 and $11.7 \times 10^{-16}$ cm$^2$ for $v = 5$ and 6, respectively.

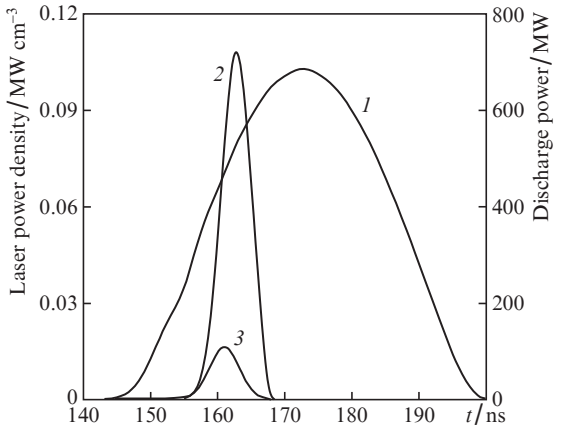


**Figure 9.** Time dependences of (*1*) the pump discharge power $P_{\mathrm{dis}}$ and intensities of (*2*) the input radiation pulse $I_0$ and (*3*) output radiation pulse $I$, obtained for $\lambda = 246.8$ nm.

Below are the results obtained for a mixture of He:Kr:$F_2$ = 2300:100:5 at a total pressure of 2.4 atm and a charging voltage of $U_0 = 22$ kV. A radiation pulse with an energy of 0.1 mJ and an FWHM of 8 ns enters the active medium in $\Delta t = 25$ ns after the discharge gap breakdown. The intensities of the input radiation pulse, the amplified radiation pulse, as well as the pump discharge power are shown in Fig. 9.

The ratio of the intensities of the input and output radiation pulses is determined by the active medium gain $g$. In the case of pulsed excitation of the active medium, the value of $g$ varies over time. Figure 10 shows the dependences of the output pulse intensity on the delay time $\Delta t$, obtained numerically and measured in the experiment. The delay time $\Delta t = 0$ corresponds to the time moment of the discharge gap breakdown. One can see a good agreement between the calculation and experimental results. The discrepancy between the curves observed at the trailing edge of the excitation pulse is associated with a deterioration in the discharge uniformity in the experiment, which is not reflected in the numerical calculation.

The maximum gain is reached earlier than the current maximum, which is typical for regimes with a high peak pump power ($n_e \approx 10^{16}$ cm$^{-3}$) due to the high rate of quenching of

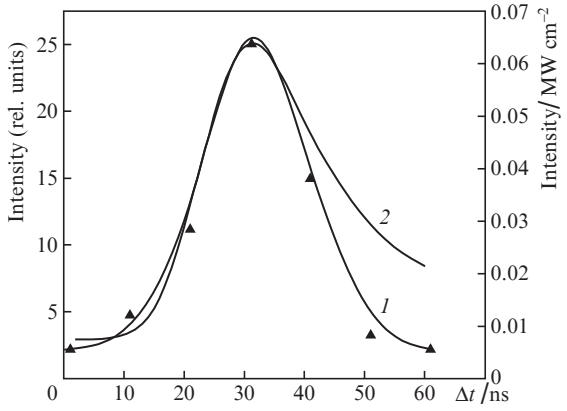


**Figure 10.** (*1*) Experimental and (*2*) calculated dependences of the output pulse intensity on the delay time $\Delta t$.

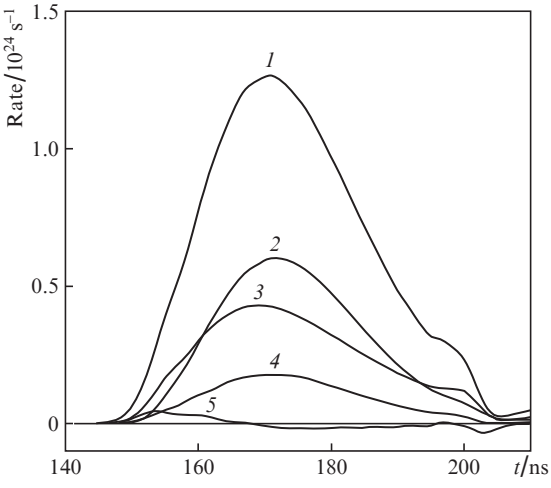


**Figure 11.** Rate of (*1*) KrF(B) molecule production, (*2*) quenching, (*3*) vibrational relaxation, and (*4*) BC exchange, as well as (*5*) total rate of change in the number of KrF (B, $v$ =100) molecules.

excimer molecules by electrons. Figure 11 shows the change during the current pulse in the rates of generation of excimer KrF(B) molecules, BC exchange, vibrational relaxation, and complete quenching of these molecules by electrons and heavy particles, as well as the rate of change in the concentration of KrF(B) molecules in the upper vibrational states. It can be seen that the rate of quenching of excimer molecules is higher than the rate of relaxation of KrF(B) molecules from upper to lower vibrational levels.

For the same conditions of active medium excitation, the medium gain $g$ was calculated for the wavelengths of 248.3 and 246.8 nm. Figure 12 shows the change in $g$ during the pump pulse action. The gain for radiation with $\lambda = 246.8$ nm is two times less than that for radiation with a centre wavelength – its maximum value is 0.05 $cm^{-1}$. This result is in good agreement with the experimentally obtained value.

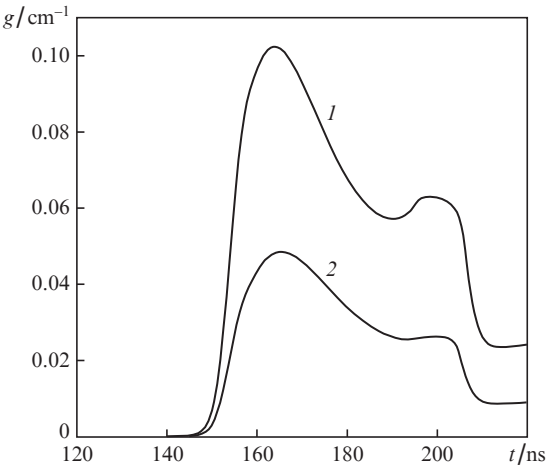


**Figure 12.** Gain for wavelengths of (*1*) 248.3 and (*2*) 246.8 nm.

## 7. Conclusions

In the present work, we have experimentally demonstrated the possibility of obtaining induced radiation during the transition from the vibrationally excited KrF(B) state to the KrF(X) state. The gain value $g = 0.053$ $cm^{-1}$ was achieved in experiments on amplification of radiation with a wavelength of 246.8 nm in the case of electric discharge excitation of a gas mixture of $He : Kr : F_2 = 2300 : 100 : 2.5$ at a total pressure of 2.4 atm by a pulse with a peak power density of 10 MW $cm^{-3}$.

The experimental results were verified by numerical calculations. The developed model was used to study the vibrational kinetics of KrF excimer molecules under conditions of pulsed pumping of the active medium. The obtained results showed that the distribution of the population of excimer molecules over vibrational levels under such conditions at pressures of 1–4 atm has a strongly nonequilibrium character. A slow decrease in the population with increasing vibrational number $v$, together with a sufficiently high efficiency of energy extraction from these levels, allows us to expect a noticeable amplification of the medium for wavelengths corresponding to optical transitions from vibrationally excited levels. This opens up new possibilities for the development of electric discharge amplifiers on excimer molecules with a tunable wavelength in the spectral range of the B–X transition band.

***Acknowledgements.*** The work was performed within the framework of the State Task (No. FWRM-2021-0014) and was supported by the Russian Foundation for Basic Research (Grant Nos 20-08-00371 and 20-58-00008-Bel_a).

## References

1. Loree T.R., Butterfield K.B., Barker D.L. *Appl. Phys. Lett.*, **32**, 171 (1978).
2. Bobrovnikov S.M., Gorlov E.V., Zharkov V.I., Panchenko Yu.N., Puchikin A.V. *Appl. Opt.*, **57**, 9381 (2018).
3. Pummer H., Hohla K., Rebentrost F. *Appl. Phys.*, **20**, 129 (1979).
4. Jacob J.H., Trainor D.W., Rokni M., Hsia J.C. *Appl. Phys. Lett.*, **37**, 522 (1980).
5. Dreiling T.D., Setser D.W. *J. Chem. Phys.*, **75**, 4360 (1981).
6. Boichenko A.M. et al. *Trudy IOFAN*, **21**, 44 (1989).
7. Kannari F., Obara M., Fujioka T.J. *Appl. Phys.*, **57**, 4309 (1985).
8. Kannari F. et al. *IEEE J. Quantum Electron.*, **QE-19**, 1587 (1983).
9. Kvaran A., Shaw M.J., Simons J.P. *Appl. Phys. B*, **46**, 95 (1988).
10. Morgan W.L., Winter N.W., Kulander K.C. *J. Appl. Phys.*, **54**, 4275 (1983).
11. Datsyuk V.V., Izmailov I.A., Kochelap V.A. *Sov. J. Quantum Electron.*, **16**, 1398 (1986) [*Kvantovaya Elektron.*, **13**, 2120 (1986)].
12. Datsyuk V.V. *Appl. Phys. B*, **55**, 60 (1992).
13. Panchenko Yu.N., Puchikin A.V., Yampolskaya S.A., Bobrovnikov S.M., Gorlov E.V., Zharkov V.I. *IEEE J. Quantum Electron.*, **57**, 1 (2021).
14. Yampolskaya S.A., Yastremskii A.G., Panchenko Yu.N., Puchikin A.V., Bobrovnikov S.M. *IEEE J. Quantum Electron.*, **56**, 1500209 (2020).
15. Smirnov B.M. *Phys. Usp.*, **20**, 119 (1977) [*Usp. Fiz. Nauk*, **121**, 231 (1977)].
16. Ongy D.S., Tou T.Y., Low K.S. *J. Phys. D: Appl. Phys.*, **29**, 2586 (1996).
17. Frost L., Phelps A. *Phys. Rev. A*, **136**, 1538 (1964).
18. Lowke J., Phelps A., Irwin B. *J. Appl. Phys.*, **44**, 4664 (1973).
19. Jacob J.H., Hsia J.C., Mangano J.A., Rokni M. *J. Appl. Phys.*, **50**, 5130 (1979).
20. Riva R., Legentil M., Pasquiers S., Puech V. *J. Phys. D: Appl. Phys.*, **28**, 856 (1995).
21. Bychkov Yu.I., Yastremskii A.G., Yampolskaya S.A., Losev V.F., Dudarev V.V., Panchenko Yu.N., Puchikin A.V. *Izv. Vyssh. Uchebn. Zaved., Ser. Fiz.*, **57**, 60 (2014).
22. Tamagake K., Setser D.W. *J. Chem. Phys.*, **67**, 4370 (1977).
23. Lo G., Setser D.W. *J. Chem. Phys.*, **100**, 5432 (1994).